JMEPEG (2015) 24:4236–4243
DOI: 10.1007/s11665-015-1738-0

1059-9495/$19.00

Characterization of GNP-Containing Al_2O_3 Nanocomposites Fabricated via High Frequency-Induction Heat Sintering Route

Iftikhar Ahmad, Mohammad Islam, Tayyab Subhani, and Yanqiu Zhu

(Submitted June 2, 2015; in revised form September 17, 2015; published online October 20, 2015)

In this paper, we present alumina (Al_2O_3) nanocomposites reinforced with various graphene nanoplatelets (GNPs) concentrations (0.75 and 1.25 wt.%) and fabricated by rapid high frequency-induction heat (HF-IH) sintering route. The influence of the GNP on the microstructures, mechanical properties, and interfacial connections of the resulting nanocomposites were thoroughly investigated. GNPs were synthesized using combined chemical oxidation and thermal exfoliation processes and dispersed homogenously into base Al_2O_3 ceramic matrix using colloidal chemistry technique. Pressure-assisted HF-IH sintering rapidly consolidated nanocomposites close to theoretical densities (~99%) without damaging the GNP intrinsic nanostructures and electron microscopy revealed firmly bonding of the nanocomposite constituents at interfaces. Nanocomposite samples containing 0.75 wt.% GNP demonstrated 60% finer microstructure with 45% higher fracture toughness (K_{IC}) and 9% improvement in hardness against benchmarked monolithic Al_2O_3. However, nanocomposites loaded with higher GNP contents (1.25 wt.%) showed deprived properties due to GNP accumulations. Homogenous dispersions and two-dimensional features allowed GNP to interact wide area of the matrix grains thus refined the microstructure and gave rise the grain anchoring mechanism thereby led nanocomposite to superior mechanical properties following GNP crack-bridging and pull-out toughening mechanisms.

Keywords Al_2O_3, graphene nanoplatelets (GNP), interface, microstructure, nanocomposite

1. Introduction

Distinctive structural and functional characteristics of the graphene are attractive for whole field of nanotechnology thereby front runners in contemporary materials (Ref 1). Graphene is two-dimensional arrangement of carbon atom and is the stiffest and strongest nanomaterials known so far. It is extremely difficult to produce monolayer graphene in high yield; however, GNP owing few graphene layers is somehow equally good and the properties of GNP suggest that polymer/ceramics matrices could be made super strong materials provided that the unique properties of GNP nanostructures could be transferred to the resulting nanocomposites (Ref 2). In this way, new stronger, stiffer, more thermally and electrically conductive materials could be realized than available today. At present, there is a great interest in multifunctional nanocomposites because these are suitable as structural materials and also satisfy the needs for additional functionality requirements such as electrical, magnetic, optical, chemical, biological, and many others (Ref 3).

Regarding structural ceramics, Al_2O_3 is an attractive for high processing industries, power generation, aerospace, transportation, and military sectors (Ref 4, 5). Currently, this promising ceramic (Al_2O_3) has applications as bearings, seals, liners, nozzles, cutting tools, dental inserts, heating elements, electrical igniters, electromagnetic/antistatic shielding of electronic components, electrode for fuel cells, crucibles for vacuum induction furnaces, electrical feed through, and cylinder lines, valve seat piston rings for automotive applications (Ref 6-8). Besides these promising applications, brittleness is the bane of Al_2O_3 ceramic and turns it down for advanced structures for aircraft engine parts, rocket materials surviving in extreme environments, armor materials for defense sector, high-temperature components for automobile and other space engineering applications (Ref 9). In this context, it is thought that newly invented nanomaterials could be a possible solution in curtaining the brittle nature of the Al_2O_3 ceramics and strong/elastic CNTs are leading among them. Both singles and multi-walled CNTs have been used to reinforce the Al_2O_3 for enhancing the fracture toughness and several reports appeared claiming success in this regard (Ref 10-18). However, severe CNTs agglomeration, inadequate nanocomposites densification, and poor interfacial connections between ceramics and CNT are big hurdles in transferring exceptional strength and elasticity of the CNT to ceramics matrices (Ref 10-22). Graphene has several advantages over CNTs such as (i) higher specific surface area, (ii) outstanding mechanical strength/flexibility, (iii) less tendency to tangle thus dispersion is far easy into a ceramic matrix than CNTs, (iv) easy to prepare in high yield, (v) economical, and (vi) less health hazards (Ref 23-25). Based on these benefits, it is postulated that the graphene could replace carbon nanotubes for preparing tougher Al_2O_3 nanocomposites

Iftikhar Ahmad and **Mohammad Islam**, Deanship of Scientific Research, Advanced Manufacturing Institute, King Saud University, P.O. Box. 800, Riyadh 11421, Kingdom of Saudi Arabia; **Tayyab Subhani**, Composite Research Center, Department of Materials Science and Engineering, Institute of Space Technology, Islamabad, Pakistan; and **Yanqiu Zhu**, College of Engineering, Mathematics and Physical Sciences, University of Exeter, Exeter EX4 4QF, UK. Contact e-mail: ifahmad@ksu.edu.sa.

but most of the work was done to improve the properties of Si_3N_4 ceramic and polymeric systems than graphene-reinforced Al_2O_3 nanocomposites. Existing literature showed fewer attempts to prepare graphene/Al_2O_3 nanocomposites, for example Walker et al. reported impressive 235% higher in fracture toughness (K_{IC}) of Si_3N_4 after loading with 1.5 vol.% graphene whereas Dusza et al. could get moderate 45% increase at 3.0 vol.% graphene additions into Si_3N_4, compared to monolithic samples (Ref 26, 27). Various workers have separately demonstrated moderate fracture toughness (K_{IC}) improvements (27, 28, 33, and 53%) in Al_2O_3 ceramic after (0.3, 0.8 vol.%, 0.22 and 2 wt.%) graphene loadings, respectively, following graphene pull-out and crack-bridging, as main toughening mechanisms. Adding on, graphene adheres well with Al_2O_3 matrix without any intermediate phase, wrapping around the Al_2O_3 grains, formed a network structure and acted as grain refiner (Ref 28-30). These reports suggest that graphene, as an effective nano-reinforcement, has improved the fracture toughness (K_{IC}) and other mechanical properties of the Al_2O_3 ceramics; however, these properties could be further pushed by using ultra-fine GNP, improving the homogenous distribution of GNP into base matrix, using novel rapid sintering process and formation of firm GNP/Al_2O_3 interface at atomic scale, thus has interesting and wide scope of research in this intriguing area of structural nanocomposites (Ref 31).

Herein, we report Al_2O_3 nanocomposites reinforced with 0.75 and 1.25 wt.% GNP concentrations and condensed through HF-IH sintering route along with systematic structural analysis and mechanical properties evaluation of the resulting nanocomposite. The aim is to (i) demonstrate novel HF-IH sintering, a promising technique for preparing dense graphene-reinforced Al_2O_3 nanocomposites which simultaneously protect graphene nanostructures from degradation and contributed in forming strong interfacial connection between GNP/Al_2O_3 for better toughness and (ii) study the effects of GNP contents on the overall microstructures and mechanical properties on the final nanocomposites.

2. Materials and Experimental Method

2.1 Nanocomposites Preparation

For GNP preparation, fine graphite flakes (grade 3775-Asbury Graphite Mills, Inc., New Jersey, USA) were first chemically modified to graphite oxide (GO) by Hummers' process and then the thermal exfoliation of the GO was performed at 1400 °C under high vacuum conditions by using heating rate of higher than 1000 °C/min (Ref 32, 33). For obtaining uniform GNP dispersions into the base Al_2O_3 matrix, an environmental friendly water-based colloidal chemistry technique was opted and for this purpose designed amounts of thermally exfoliated GNP (0.2 g) were added into distilled water (100 mL) and small amount of sodium dodcyle sulfate (SDS, <2 wt.% of the graphene nanoplatelets—GNPs) was also added. The aqueous GNP/SDS slurry was then agitated with the assistance of ultra-sonic probe (Sonic Vibracell, VCX-750, manufactured by Sonics,Materials Incorporation, USA, power 750 watts, frequency 20 kHz) for 30 min and sufficient time (2 week) was given to slurry for thorough adsorption of SDS on the GNP surfaces and resonicated for 30 min. A separate slurry of aqueous/Al_2O_3 nanopowder (Sigma Aldrich, UK having particle size <50 nm, gamma phase <50 nm, BET surface area >40 m^2/g) was also prepared and later both suspensions were mixed each other and ultrasonicated for 60 min and dried at 120 °C. The dried nanocomposite mixtures were then condensed by HF-IH sintering furnace (HF Active Sinter System, ELTEK, Korea). All samples were processed at fixed HF-IH sintering parameters i.e., sintering temperature 1500 °C, heating rate of 150 °C/min, dwell time of 3 min, an uniaxial pressure of 50 MPa and high vacuum (4.5×10^{-2} Tor). Moreover, the sintering temperatures of whole consolidation process were consistently monitored by an optical pyrometer (Thermalert TX, Raytek GmbH, Germany). Pure monolithic Al_2O_3 reference samples were also fabricated following the similar processing conditions.

2.2 Physical Properties and Material Characterization

To measure the apparent densities of all sintered samples, a well-known Archimedes method was adopted. For relative density assessment, the theoretical densities of 3.97 g/cm^3 for Al_2O_3 and 2.10 g/cm^3 for GNP were used (Ref 26, 34). Bruker D-8 Discover x-ray diffractometer using Cu Kα radiation, Germany was utilized to identify the phases present in the sintered samples. Structural features and grain size were analyzed by scanning electron microscope, SEM, (FEG-SEM JEOL JSM-7600F, Japan). Fractured and polished/thermally etched samples, at 1400 °C for 15 min in inert atmosphere, were prepared for observation under SEM. For structural examination of GNPs and interfacial investigations of the GNP/Al_2O_3 nanocomposites, an advanced transmission electron microscope, TEM, (FEG-TEM 2100F, JEOL, Japan) was used. For TEM analysis, GNP sample was prepared by dispersing GNP into acetone and later transferred to holey-carbon TEM grid. For interfacial investigation, sintered nanocomposite samples were prepared by ion milling technology using ion-slicer (EM 09100 IS, JEOL, Japan).

2.3 Mechanical Testing

Microhardness of all polished sintered samples were measured at 9.8 N loads for 15 s employing Buehler-micromet 5114 (Akashi corporation, Japan) and later the obtained Vickers hardness numbers (HV) were further converted to GPa (Ref 21). Nanoindentation technique was adopted to determine the nanohardness and elastic modulus of all sintered samples. Nanoindentation measurements were performed using a NanoTest, (Micro Materials, and UK). The indenter was continuously loaded to peak load of 200 mN in 25-30 s and unloaded after holding time of 30 s to allow full plastic deformation. Reduced modulus was directly obtained from machine whereas the modulus of elasticity was calculated by employing Eq 2 (Ref 35)

$$E = \frac{\left[1 - V_s^2\right]}{\left[\frac{1}{E_r} - \frac{\left\{1 - V_i^2\right\}}{E_i}\right]}, \qquad \text{(Eq 1)}$$

where V_s and V_i are the Possion's ratio of the test piece (0.23 for monolithic Al_2O_3 and composites) and the indenter (0.07 for diamond), respectively, E_i is the elastic modulus of the indenter (1.14×10^6 Nm/m^2 for diamond).

The toughness of all nanocomposites was appraised using the direct crack measurement (DCM) method, the lengths of

crack emerging from the corner of an indent generated during Vickers hardness tests were used to estimate the K_{IC}. The crack lengths were carefully measured using SEM and the recorded images were analyzed using images processing and analysis software (ImageJ). The K_{IC} value was calculated using Eq 2 (Ref 36)

$$K_{IC} = 0.016\left(\frac{E}{H}\right)^{\frac{1}{2}}\left(\frac{P}{C^{\frac{3}{2}}}\right), \quad \text{(Eq 2)}$$

where E is the modulus of elasticity, H is the micro-hardness (HV) and c is the radial crack length generated by the Vickers indentation. 10 indents were made on each sample.

3. Results and Discussions

3.1 GNP Synthesis and Dispersions

Figure 1 provides two important structural details, obtained from combined electron microscopy, demonstrating the quality of the (i) GNP prepared by combined processing and (ii) homogenous GNPs dispersion within the base Al_2O_3 matrix. Figure 1(a) shows SEM image of the thermally exfoliated GNP where stacks of two-dimensional platelet-like geometrical features can be identified and the close observation of an edge of a single GNP has nanometer dimension, as shown in Fig. 1(b). Furthermore, light contrast of the same GNP sample under TEM portrays thin or mono GNP whereas relatively darker contract represents fewer GNP layers and the crumpling or wrinkling of thin GNP were also observed as exhibited in Fig. 1(c). These microscopic details indicate that the GNP has sustaind severe chemical processes and complex physical activities during preparation despite, the GO has to undergone stern chemical processes (eradication of the H_2O molecules and oxides groups intercalates) and rigorous physical phenomenon (folding/unfolding of the graphene layers and reshuffling of graphene layers at the instant of rapid thermal shock) prior to its transformation into thin GNP (Ref 37). These obvious microscopic images suggest that GNP has successfully resisted against degradation thus maintaining its two-dimensional platelet morphology, structure and nanoscale features.

To transfer the intrinsic properties of GNP, an even distribution of the GNPs within the Al_2O_3 grains is an essential step to obtain superior quality nanocomposites. SEM fractured surfaces of the sintered samples in Fig. 2(b) clearly show the homogenous distribution of the GNPs (white arrows) within the Al_2O_3 grains. Indeed combined processing of ultrasonication, surfactant and time provided for surfactant adsorption to GNP surfaces jointly contributed in obtaining the uniform distribution of GNPs within the parent ceramic matrix. Indeed, ultrasonication has provided high energy sonic waves to detangle the GNPs and the surfactant adsorbed on the GNP surfaces has created positive electrostatic repulsive force with each others to counter the Van der Waal attractions between GNP layers for even distributions of the GNPs within Al_2O_3 microstructure, as already reported (Ref 26).

3.2 Densification and Structural Features

Figure 3(a) represents that the novel HF-IH sintering has consolidated monolithic Al_2O_3 to near theoretical densities (99.5%); however, a minor decrease of 0.5% was observed in

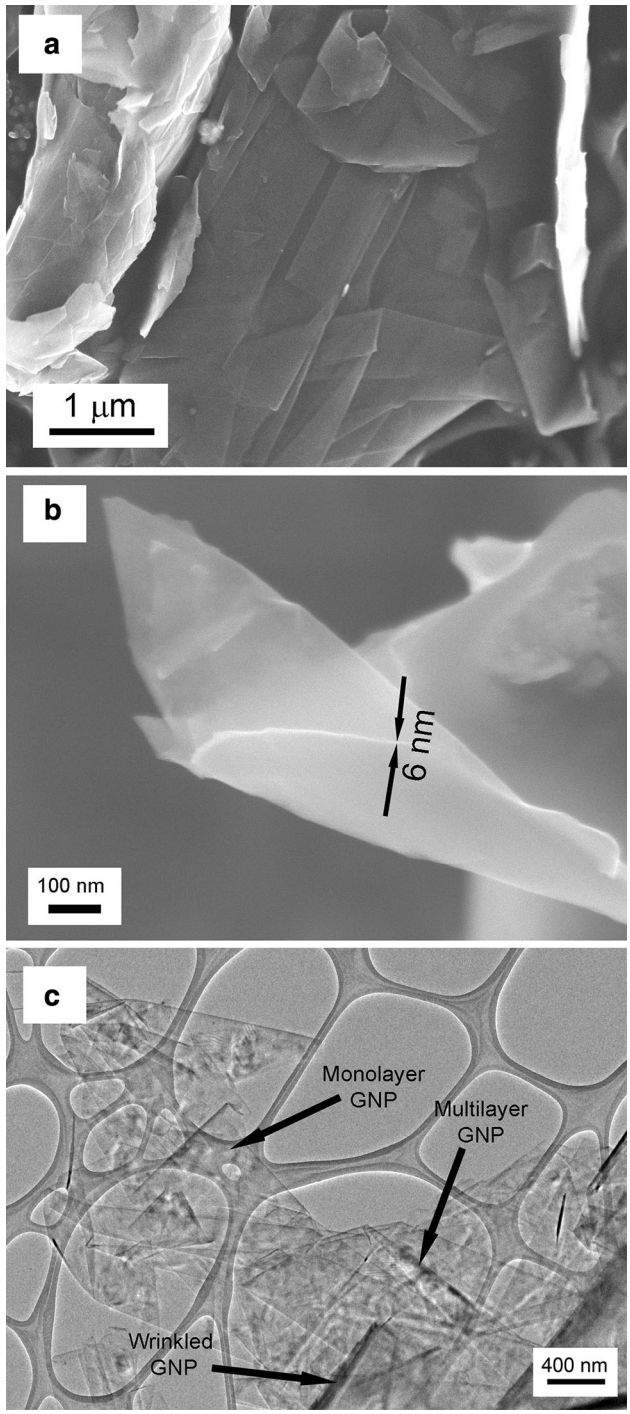

Fig. 1 SEM images of thermally exfoliated GNP at (a) low magnification, showing stacks of GNP, (b) high magnification, showing the GNP cross section and (c) TEM image of thermally exfoliated GNP depicting monolayers, few layered and wrinkled features

the density of the nanocomposite loaded with 0.75 wt.% GNP, whereas nanocomposite samples containing 1.25 wt.% GNP could show a relative density of 96%. These results indicate that novel HF-IH sintering technique, owning rapid heating rate, simultaneous pressure application and short sintering duration, is promising to condense GNP/Al_2O_3 nanocomposites to higher densities (Ref 38). The novel HF-IH sintering process was carried out by placing the nanocomposite powered inside a

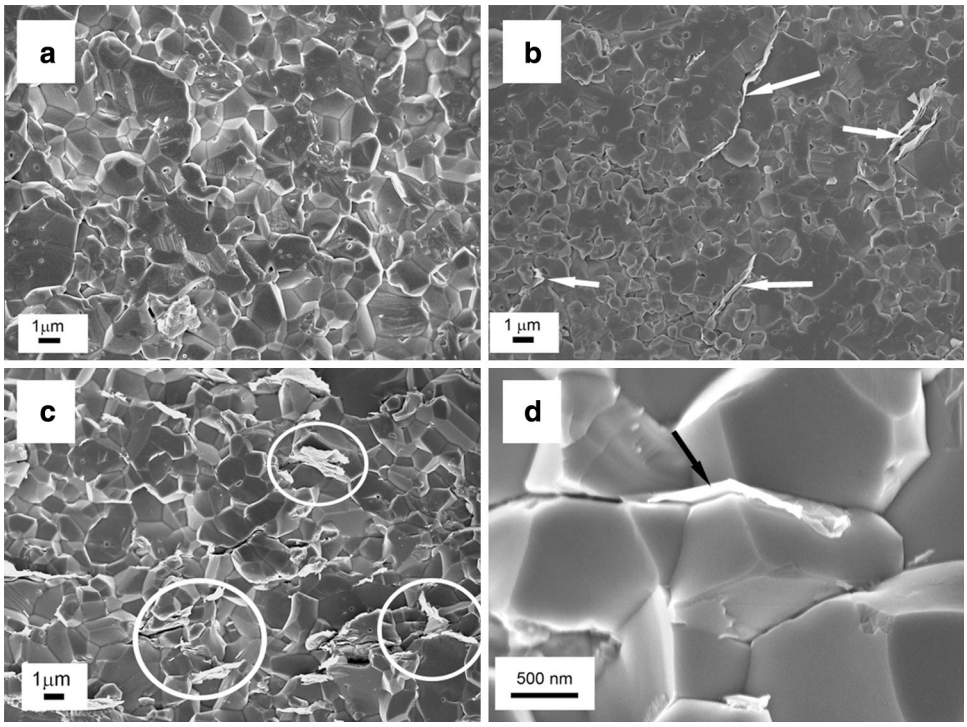

Fig. 2 SEM images of the fractured samples of (a) monolithic Al_2O_3, (b) Al_2O_3-0.75 wt.% GNP nanocomposites samples showing the homogenous dispersions of GNP (white arrows), (c) GNP gluts (white circles) in Al_2O_3-1.25 wt.% GNP nanocomposites and (c) wrapping of GNP (black arrow) around Al_2O_3 matrix grains

graphite mold cavity, somehow like hot-pressing, and the graphite mold was heated by a source of high-frequency electricity to drive a large alternating current through a copper (Cu) induction coil, around the graphite mold, as schematically illustrated in Fig. 3(b). In principle, the current carrying induction generates highly intense and rapidly changing magnetic field in the space within the induction coil. The conductive graphite mold containing ceramic composite powder is placed within this intense alternating magnetic field which induces a current flow in the conductive graphite die. Thus allows the right amount of heat for desired period of time which surely ensures controlled performance without damaging the GNPs nanostructure and consolidate nanocomposite to higher densities (Ref 39). Moreover, the uniform dispersions of GNP within parent matrix are also important and Fig. 2b shows that the water-based colloidal technique efficiently distributed GNPs into Al_2O_3 matrix thus allowed matrix nanoparticles to coalescence for better densification. Nanocomposites were prepared with high GNP concentrations (1.25 wt.%); however, it exhibited GNP gluts at matrix grain boundaries (Fig. 2c) thus deprived (96%) densification level, as shown Fig. 3(a).

In Fig. 3(c), the XRD pattern of all sintered samples exhibits characteristic crystalline peaks of Al_2O_3 matching JCPDS card No. 01-078-2426; however, a new peak was recognized at 26.3° in nanocomposite samples corresponding to the crystalline graphite according to JCPDS No. 01-075-1621. Figure 2 also demonstrates that interesting details about the interaction of GNPs with Al_2O_3 matrix and the nature of fracture-mode, deboning of GNP, pulled-out GNP from the ceramic matrix (Fig. 2b), and wrapping of ceramic matrix grains by GNP (Fig. 2c) are clearly visible in the SEM images of the fractured nanocomposites. Although grain refinement is another advantage of rapid HF-IH sintering technique due to short sintering duration compared to long hours hot-pressing (Ref 21) and the GNPs further refined the microstructure of base matrix by pinning the grain boundaries, thus the Al_2O_3-0.75 wt.% GNP nanocomposite sample exhibited smaller grains (600 nm) compared to 1.5 μm grain size of the monolithic Al_2O_3, as demonstrated in Fig. 3(a) and 4(b). In contrast, higher additions merely influence the grain size of nanocomposite other than increasing the concentration of the GNPs at grain boundaries, as shown in Figs. 3(a). Indeed, GNP has tendency to be distributed between ceramic grains boundaries and prevented the migration of grain boundaries, resulting in a refinement of microstructure, as structurally shown in Fig. 4. Figure 2(d) also shows that the GNPs are wrapped around (black arrow) the matrix grain boundaries and this might be another reason behind the grain refinement effect in the nanocomposites because GNP existing around the grain boundaries can effectively prevent the grain growth during sintering, and can act as pining points to stop grain boundary movement during grain growth during consolidation process (Ref 28).

3.3 Fracture Toughness (K_{IC}) and Other Mechanical Properties

Fracture toughness values are graphically represented in Fig. 5(a), which shows that Al_2O_3-0.75 wt.% nanocomposites demonstrated a K_{IC} value of 4.5 MPa.m$^{1/2}$ which is 45% higher than the benchmark monolithic Al_2O_3 (3.1 MPa.m$^{1/2}$), whereas nanocomposites reinforced with 1.25 wt.% GNP hardly showed improvements in the K_{IC} value (3.3 MPa.m$^{1/2}$). In this study, the K_{IC} values of all samples were determined using direct crack method (DCM) and this technique is less reliable than standard monolithic SENB (Single-edge notch beam) method however used in several studies, to assess the K_{IC}

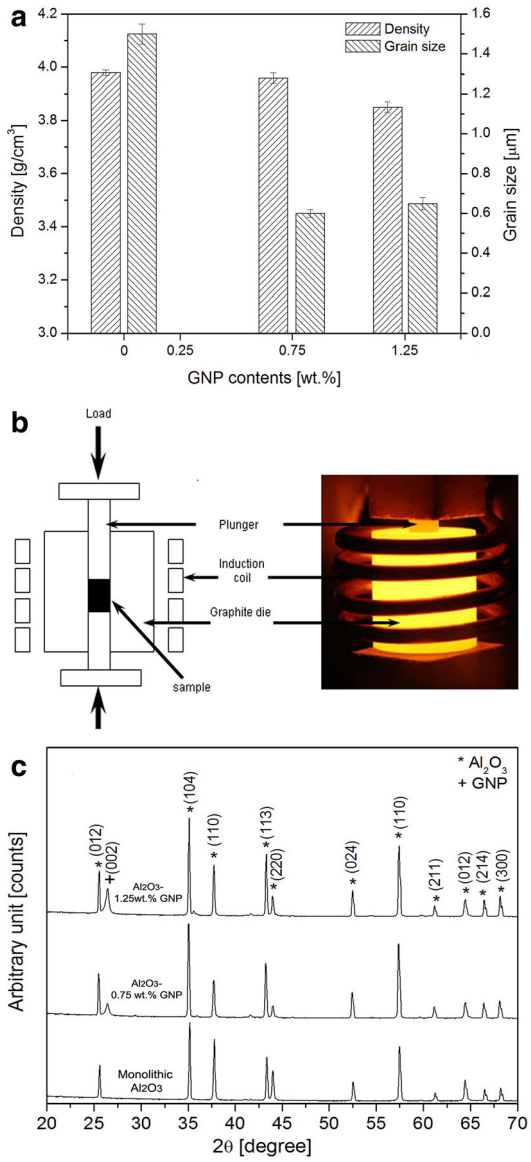

Fig. 3 (a) Density and grain size profiles of monolithic Al_2O_3 as function of GNP additions, (b) schematic illustration of the HF-IH sintering process and (c) XRD profiles of all sintered samples

values of monolithic ceramics and nanocomposites (Ref 13, 16, 18-20).

Analysis of the fractured surfaces using SEM provided useful details which explain the probable reasons behind the hike in the K_{IC} values. Figure 6(a) shows GNP pull-out in the freshly fractured nanocomposites samples; thus, it can be deduced that the conventional toughening mechanisms derived for fiber reinforced composites could be applied to Al_2O_3-GNP nanocomposites (Ref 21). Moreover, toughening mechanism of GNP grain sharing (Fig. 6a) and crack bridging were also noticed in the nanocomposite (Fig. 6b), and these toughening mechanisms seem to contribute in improving K_{IC} in the nanocomposites.

It is seen in Fig. 6(a) that the GNP is perfectly embedded within the two Al_2O_3 grains thus strengthening the grain boundaries and leading to the change in the fracture mode, from inter-granular in case of monolithic Al_2O_3 (Fig. 2a) to mixed trans-transgranular in the nanocomposites (Fig. 2b). Further, Fig. 2d shows that a large GNP securely was wrapped/rolled around the Al_2O_3 grain (black arrow), possibly due to their flexibility and high aspect ratio, forming a large area of interface with matrix. This unique interaction associated with the two-dimensional geometry of the GNP generated anchoring mechanism (TEM image Fig. 7a, white arrow), which can lead to increased interfacial frictions between the GNP and the matrix, and increase the required energy to pull-out such GNPs (Ref 40). Therefore, the fracture accrued through the Al_2O_3 grains rather than grain boundaries, as demonstrated in Fig. 2(b). These results mean that the GNPs have played a significant role in improving the fracture toughness, due to their distinctive microstructures by (i) increasing the required pull-out energy during fracture (ii) anchoring around the Al_2O_3 grains and (ii) producing higher contact area with matrix grains.

Figure 5(b) represents 9% increase in the hardness values of the nanocomposite containing 0.75 wt.% GNP; however, 12% drop in hardness was noticed in nanocomposites containing 1.25 wt.% GNP contents, against reference monolithic Al_2O_3. Nanocomposites exhibited elastic modulus values of 390 and 370 MPa for respective GNP loadings of 0.75 and 1.25 wt.%, which are 8 and 13% higher than the reference monolithic Al_2O_3 (426 MPa), as shown in Fig. 5(b). It is well known that the hardness of the ceramic materials largely depends on the grain size and grain morphology thus any modifications in these two important microstructural parameters could influence

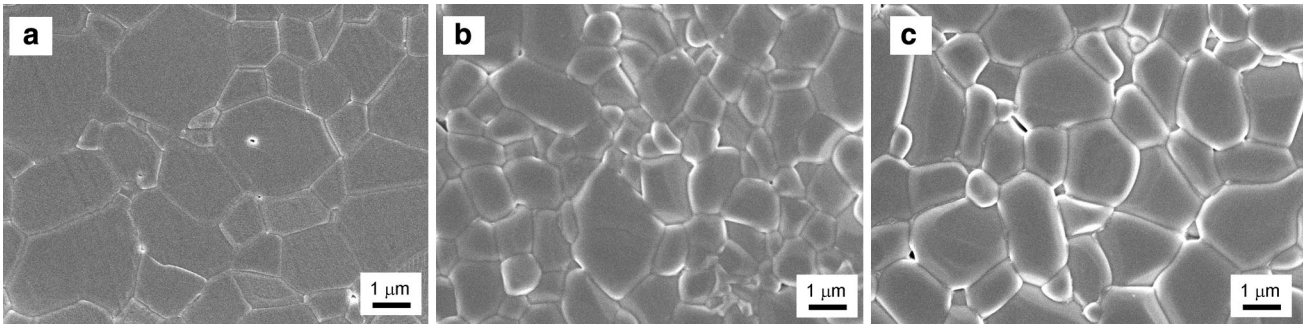

Fig. 4 SEM images of the thermally etched (a) monolithic Al_2O_3 and nanocomposites reinforced with GNP concentrations of (b) 0.75 wt.% and (c) 1.25 wt.%

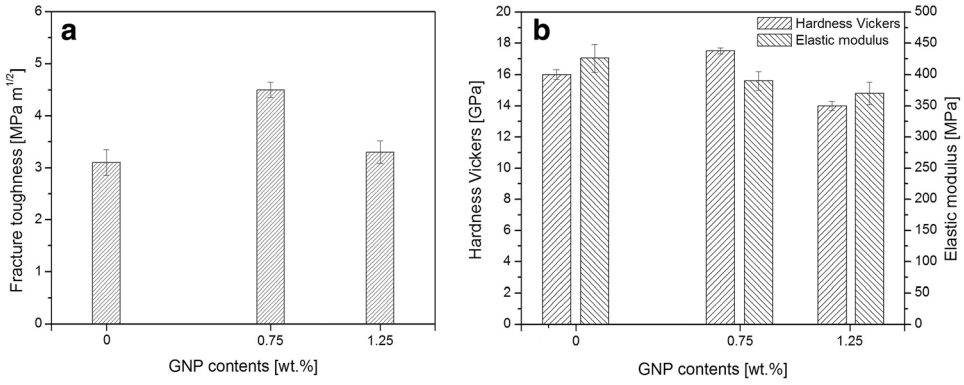

Fig. 5 Effects of GNP contents on the (a) fracture toughness and (b) hardness and elastic modulus of the monolithic Al_2O_3

the hardness values (Ref 41). Microstructure of the monolithic Al_2O_3 (Fig. 4a) showed elongated prismatic, acicular or needle-like grain shapes and this could be potential reason for high hardness values (Ref 12-14). In contrast, the nanocomposites exhibited fined-grain macrostructure after 0.75 wt.% GNP addition indicating that the GNP has refined the microstructure by pinning the grain boundaries, as shown in Fig. 4(b). Indeed, the grain boundaries and reinforcing constituents hinder the onset of plasticity and impede the dislocation movements across the entire nanocomposite microstructures; hence, 9% hike in the hardness value was obtained in nanocomposite sample loaded with 0.75 wt.% GNP concentration, compared to monolithic Al_2O_3 fabricated under the same conditions (Ref 20, 41). On the other hand, a 12% hardness reduction was noticed in nanocomposite having 1.25 wt.% GNP contents and this decrease in hardness value, against monolithic Al_2O_3, may be associated with the apparent changes in the grain morphology and graphene intrinsic lubrication characteristics (Ref 42). Blunt grain morphology appearance in Fig. 4(c) could probably be leading reason in the hardness drop because it is possible that blunt-shaped grains may have facilitated the deformation/sliding of grains on each other, as the rounded one obviously slides far easily than faceted one (Ref 42). Moreover, a consistent decrease in the elastic modulus of the nanocomposite with increasing GNP contents was also noticed, as represented in Fig. 5(b). In this regard, Fan et al. reported that the grain size barley influenced the elastic modulus; however, low modulus of the GNP in both in-plane and out-of-plan directions could likely be the leading reasons behind lowering the elastic modulus in the nanocomposite samples (Ref 42).

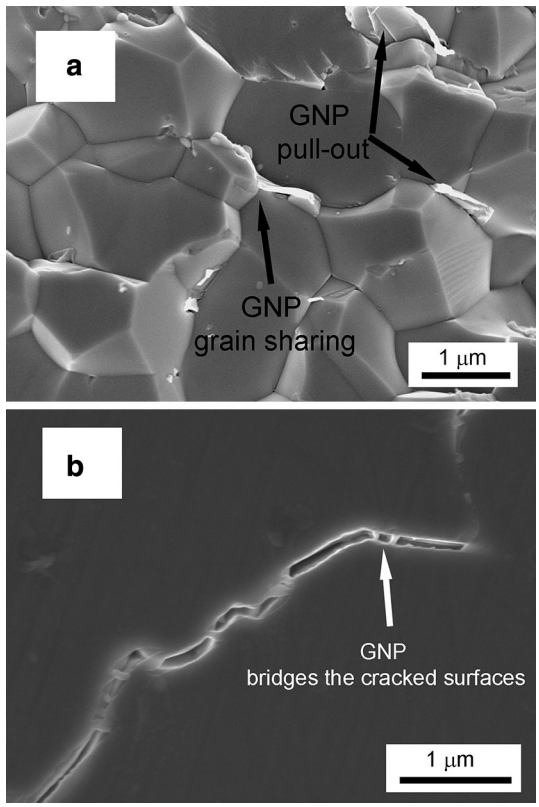

Fig. 6 High-resolution SEM images of the nanocomposite (a) fractured surface exhibiting GNP pull-out, grain sharing and (b) shows GNP bridging the cracked surfaces

3.4 Interfacial Investigations

In nanocomposite, the Al_2O_3/GNP interface plays a vital role to transfer the exceptional mechanical properties of GNP to the nanocomposite thus helpful in performing toughening mechanism. It is obvious that weakly bonded GNP would pull-out easily from Al_2O_3 matrix during loading sequence; hence, would be unable to transport stress from one Al_2O_3 grain to another, and this could lead nanocomposite to meager mechanical performance. To study the Al_2O_3/GNP interface, the interfacial details that exist at Al_2O_3/GNP junctions were revealed with the help of high-resolution TEM. Low magnification TEM image, Fig. 7(a), provides that the GNPs are homogenously dispersed within matrix grains and are located preferentially at grain boundaries. Furthermore, Fig. 7(b) shows high-resolution lattice resolved TEM images of the nanocomposite, where the GNP with typical fringe separation of 0.34 nm corresponds to the graphitic (002) planes of GNPs can be indentified and Al_2O_3 can also be recognized by its fridge distance of 0.34 nm corresponding (012) planes. In earlier studies, the formation of a strong connection at the Al_2O_3/CNT interface through an intermediate thin phase (Al_2OC) has been reported (Ref 18, 19). Nevertheless, both the CNT and GNP are constituted by graphitic structure; however, our FEG-TEM investigation reveals that GNP is directly adhere with the Al_2O_3 without any severe intermediate phases. The reported interface in case of Al_2O_3/CNT is probably due to the long duration sintering process i.e., hot-pressing which may have allowed CNT/Al_2O_3 to form an intermediate phase through slow diffusion mechanism (Ref 18).

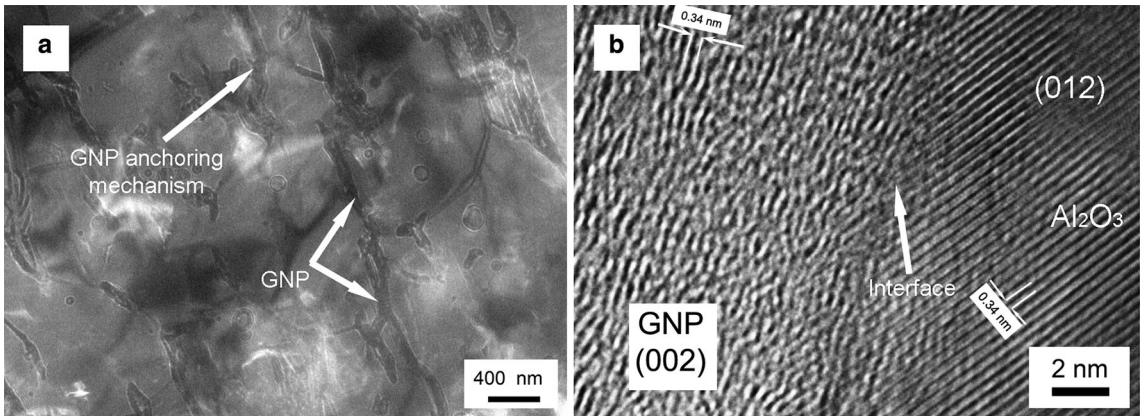

Fig. 7 (a) Low magnification TEM image of the nanocomposites shows interaction of GNP with matrix and (b) lattice resolved HR-TEM image of the nanocomposite depicting the Al_2O_3/GNP interface

In contrast, novel HF-IH technology adopted in this study is a rapid sintering technology and the sintering mechanism is entirely different (creep and related mechanisms) from the conventional (diffusion and mass transportation of materials across grain boundaries) sintering processes (Ref 18, 38, 39). Based on these TEM details, it may be stated that the strong GNP/Al_2O_3 interfacial connections may have allowed GNP to play a direct contribution in absorbing more energy during crack propagations and facilitated GNP to utilize its intrinsic elasticity and other mechanical traits during grain anchoring, pull-out and crack-bridging toughening mechanisms; thus it led nanocomposite to higher K_{IC} values.

4. Conclusions

In this report, we used novel rapid high-frequency induction-heat (HF-IH) sintering technology to fabricate Al_2O_3 (alumina) ceramic nanocomposites reinforced with 0.75 and 1.25 wt.% GNP contents. The resulting nanocomposites were appraised for structural investigations, interface and mechanical properties employing diverse analytical techniques. The graphite flakes were chemically reduced to prepare graphite oxide (GO) and then transferred to thin GNP by combined chemical/thermal exfoliation processes, and the electron microscopy confirmed the preparation of very thin (~6 nm) GNPs. Later these GNPs were evenly distributed into Al_2O_3 ceramic matrix opting colloidal chemistry method. HF-IH sintering consolidated monolithic Al_2O_3 to near theoretical densities (3.98 g/cm^3); however, a minor decrease of 0.5% was observed in the densities of the nanocomposites (3.96 g/cm^3) loaded with 0.75 wt.% GNP. In contrast, nanocomposite samples containing 1.25 wt.% GNP could be condensed to lower density (3.85 g/cm^3), due to GNP accumulations. New HF-IH sintering route, practiced in this study, provided several benefits such as (i) condensed the monolithic Al_2O_3 and nanocomposites to higher sintered densities, (ii) short sintering duration protected the nanostructures of GNP from degradation by retaining its morphology/structure, and (iii) contributed in forming strong Al_2O_3/GNPs interfacial connections. Structurally, 60% and 55% refinement into the grain size of monolithic Al_2O_3 was obtained at the GNP loading of 0.75 vol.% and 1.25 wt.%, respectively, and the incorporation of GNP also altered the fracture mode from intergranular in monolithic Al_2O_3 to mixed transgranular in the nanocomposites. Mechanically, the K_{IC} and hardness values were increased to 45% and 9% for nanocomposites having 0.75 wt.% GNP, against monolithic Al_2O_3 sample, whereas the nanocomposite containing higher GNP concentrations hardly showed any improvements due to severe GNP gluts. Rise in the K_{IC} values and hardness of the nanocomposites were associated with the (i) higher densities due to novel HF-IH sintering, (ii) uniform dispersions of the GNP within Al_2O_3 matrix, (iii) fracture-mode alteration, (iv) grain refinement, (v) strong GNP/Al_2O_3 interface, and (vi) grain bridging, sharing, anchoring toughening mechanism in GNP/Al_2O_3 nanocomposites.

Acknowledgments

The authors would like to extend their sincere appreciation to the Deanship of Scientific Research at King Saud University for its funding of this research through the Research Group Project No. RGP-VPP-283.

References

1. K.S. Novoselov, A.K. Geim, S.V. Morozov, D. Jiang, Y. Zhang, S.V. Dubonos, I.V. Grigorieva, and A.A. Firsov, Electric Field Effect in Atomically Thin Carbon Films, *Science*, 2004, **306**, p 666–669
2. S. Bai and X. Shen, Graphene-Inorganic Nanocomposites, *RSC Adv.*, 2012, **2**, p 64–98
3. H. Shifeng and C. Xin, Effect of Carbon Black on Properties of 0-3 Piezoelectric Ceramics/Cement Composites, *Curr. Appl. Phys.*, 2009, **9**, p 1191–1194
4. K. Niihara, New Design Concept of Structural Ceramics-Ceramics Nanocomposites, *J. Ceram. Soc. Jpn.*, 1999, **99**, p 974–982
5. A. Centeno, V.G. Rocha, B. Alonso, A. Fernández, C.F. Gutierrez-Gonzalez, R. Torrecillas, and A. Zurutuza, Graphene for Tough and Electroconductive Alumina Ceramics, *J. Eur. Ceram. Soc.*, 2013, **33**, p 3201–3210
6. Y. Wu, X. Zhang, and J. Guo, Microstructural Development and Mechanical Properties of Self-Reinforced Alumina with CAS Addition, *J. Eur. Ceram. Soc.*, 2001, **2**, p 581–587
7. G. Evans, Perspective on the Development of High-Toughness Ceramics, *J. Am. Ceram. Soc.*, 1990, **73**, p 187–206
8. J.R. Martinlli and F.F. Sene, Electrical Resistivity of Ceramic-Metal Composite Materials: Application in Crucibles for Induction Furnaces, *Ceram. Int.*, 2000, **26**, p 325–335

9. L. Osayande and I. Okoli, Fracture Toughness Enhancement for Alumina System: A Review, *Int. J. Appl. Ceram. Technol.*, 2008, **5**, p 313–323
10. J. Llorca, M. Elices, and J.A. Celemin, Toughness and Microstructural Degradation at High Temperature in SiC Fiber-Reinforced Ceramics, *Acta Mater.*, 1998, **46**, p 2441–2453
11. F. Yongqing, Y.W. Gu, and D. Hejun, SiC Whisker Toughened Al_2O_3-(Ti, W)C Ceramic Matrix Composites, *Scr. Mater.*, 2001, **44**, p 111–116
12. D.E. Garcıa, S. Schicker, J. Bruhn, R. Janssen, and N. Claussen, Processing and Mechanical Properties of Pressureless-Sintered Niobium-Alumina-Matrix Composites, *J. Am. Ceram. Soc.*, 1998, **81**, p 429–432
13. N. Padture, Multifunctional Composites of Ceramics and Single-Walled Carbon Nanotubes, *Adv. Mater.*, 2009, **21**, p 1767–1770
14. Tougher. Peigney, Ceramics with Nanotubes, *Nat. Mater.*, 2003, **2**, p 15–16
15. J. Fan, D. Zhao, and J. Song, Preparation and Microstructure of Multi-walled Carbon Nanotubes Toughened Al_2O_3 Composite, *J. Am. Ceram. Soc.*, 2006, **89**, p 750–753
16. C. Laurent, A. Peigney, and A. Rousset, Carbon Nanotubes-Fe-Alumina Nanocomposites: Part II: Microstructure and Mechanical Properties of the Hot-Pressed Composites, *J. Eur. Ceram. Soc.*, 1998, **18**, p 2005–2013
17. G. Zhan, J. Kuntz, J. Wan, and K. Mukherjee, Single-Walled Carbon Nanotubes as Attractive Toughing Agent in Alumina Based Nanocomposites, *Nat. Mater.*, 2003, **2**, p 38–42
18. S. Sarkar and P.K. Das, Microstructure and Physicomechanical Properties of Pressure-Less Sintered Multi-walled Carbon Nanotube/Alumina Nanocomposites, *Ceram. Int.*, 2012, **38**, p 423–432
19. I. Ahmad, A. Kennedy, and Y.Q. Zhu, Carbon Nanotubes Reinforced Alumina Nanocomposites: Mechanical Properties and Interfacial Investigations, *J. Compos. Sci. Technol.*, 2010, **70**, p 1199–1206
20. F. Inam, T. Pijis, and M.J. Reece, The Production of Advanced Fine-Grained Alumina by Carbon Nanotubes Addition, *J. Eur. Ceram. Soc.*, 2011, **31**, p 2853–2859
21. I. Ahmad, H. Cao, H. Chen, H. Zhao, A. Kennedy, and Y.Q. Zhu, Carbon Nanotube Toughened Aluminium Oxide Nanocomposites, *J. Eur. Ceram. Soc.*, 2009, **30**, p 865–873
22. I. Ahmad, A. Kennedy, and Y.Q. Zhu, Wear Resistance Properties of Multi-walled Carbon Nanotubes Reinforced Al_2O_3 Nanocomposite, *Wear*, 2010, **26**, p 971–978
23. Y.C. Fan, L.J. Wang, J.L. Li, J.Q. Li, S.K. Sun, F. Chen, L.D. Chen, and W. Jiang, Preparation and Electrical Properties of Graphene Nanosheet/ Al_2O_3 Composites, *Carbon*, 2010, **48**, p 1743–1749
24. T. He, J.L. Li, L.J. Wang, J.J. Zhu, and W. Jiang, Preparation and Consolidation of Alumina/Graphene Composite Powders, *Mater. Trans.*, 2009, **50**, p 749–751
25. C.W. Lam, J.T. James, R. McCluskey, S. Arepalli, and R.L. Hunter, A Review of Carbon Nanotube Toxicity and Assessment of Potential Occupational and Environmental Health Risks, *Crit. Rev. Toxicol.*, 2006, **36**, p 189–217
26. L.S. Walker and E.L. Corral, Toughness in Grapheme Ceramic Composites, *ACS Nano*, 2011, **4**, p 3182–3190
27. J. Dusza and C. Balaszi, Microstructure and Farcture Toughness of Si_3N_4 + GNP Platelet Composites, *J. Eur. Ceram. Soc.*, 2012, **32**, p 3389–3397
28. K. Wang and T. Wei, Preperation of Graphene Nanosheets/Alumina Composites by Spark Plasma Sintering, *Mater. Res. Bull.*, 2011, **46**, p 315–318
29. L. Jain and H.K. Jiang, Mechanical Properties of Graphene Platelets-Reinforced Alumina Ceramics Composites, *Ceram. Int.*, 2013, **39**, p 6215–6221
30. H. Porwal, P. Tatarko, S. Grasso, J. Khaliq, I. Dlouhy, and M.J. Reece, Graphene Reinforced Alumina Nano-Composites, *Carbon*, 2013, **64**, p 359–369
31. H. Porwal, S. Grasso, and M.J. Reece, Review of Graphene-Ceramic Matrix Composites, *Adv. Appl. Ceram.*, 2013, **112**, p 443–454
32. W.S. Hummers and R.E. Offeman, Preparation of Graphitic Oxide, *J. Am. Chem. Soc.* , 1958, **80**, p 1339
33. S. Pei and H. Cheng, The Reduction of Graphene Oxide, *Carbon*, 2012, **50**, p 3210–3228
34. I. Ahmad, M. Islam, A.A. Almajid, B. Yazdani, and Y.Q. Zhu, Investigation of Yttria-Doped Al_2O_3 Nanocomposites Reinforced by Multi-walled Carbon Nanotubes, *Ceram. Int.*, 2014, **40**, p 9327–9335
35. A. Chorfa, M.A. Madjoubi, M. Amidouche, N. Bouras, J. Rubio, and F. Rubiom, Glass Hardness and Elastic Modulus Determination by Nanoindentation Using Displacement and Energy Methods, *Ceram. Silik.*, 2010, **54**, p 225–234
36. G.R. Anstis, P. Chantikul, and D.B. Marshal, A Critical Evaluation of Indentation Technique for Measuring Fracture Toughness: I. Direct Crack Method, *J. Am. Ceram. Soc.*, 1981, **64**, p 533–538
37. H.C. Schniepp, J.L. Li, M.J. McAllister, H. Sai, M. Herrera-Alonso, D.H. Adamson, R.K. Prudhomme, R. Car, D.A. Saville, and I.A. Aksay, Functionalized Single Graphene Sheets Derived from Splitting Graphite Oxide, *J. Phys. Chem. B*, 2006, **11**, p 8535–8539
38. H.C. Kim, D.Y. Oh, and I.J. Shon, Sintering of Nanophase WC-15 vol.% Co Hard Metals by Rapid Sintering Process, *Int. J. Refract. Hard Mater.*, 2004, **22**, p 197–203
39. S.W. Kim and K.A. Khalil, High-Frequency Induction Heat Sintering of Mechanically Alloyed Alumina–Yttria-Stabilized Zirconia Nanobioceramics, *J. Am. Ceram. Soc.*, 2006, **89**, p 1280–1285
40. B. Yazdani, Y. Xi, I. Ahmad, and Y.Q. Zhu, Graphene and Carbon Nanotube (GNT)-Reinforced Alumina Nanocomposites, *J. Eur. Ceram. Soc.*, 2015, **35**, p 179–186
41. I. Ahmad, M. Islam, F. Xu, S.I. Shah, and Y.Q. Zhu, Magnesia Tuned Multi-walled Carbon Nanotubes-Reinforced Alumina Nanocomposites, *Mater. Character.*, 2015, **99**, p 210–219
42. Y. Fan, M. Estili, G. Igarashi, and A. Kawasakia, The Effect of Homogeneously Dispersed Few-Layer Graphene on Microstructure and Mechanical Properties of Al_2O_3 Nanocomposites, *J. Eur. Ceram. Soc.*, 2014, **34**(2), p 443–451